Clim Dyn (2015) 45:1859–1875
DOI 10.1007/s00382-014-2439-3

Influences of ENSO on the vertical coupling of atmospheric circulation during the onset of South Asian summer monsoon

Boqi Liu · Guoxiong Wu · Roncai Ren

Received: 10 May 2014 / Accepted: 8 December 2014 / Published online: 23 December 2014

Abstract Based on multiple sources of atmospheric and oceanic data, this study performs a series of composite analysis of the South Asian summer monsoon (SASM) onset against ENSO events, and indicates that warm/cold ENSO events induce later/earlier onset of the SASM by modulating the vertical coupling of the upper- and lower-level circulation over the South Asia. Specifically, during the monsoon onset of Bay of Bengal (BOB), the ENSO-induced convection anomalies over the southern Philippines can modulate the position of South Asian high (SAH) in late April in the upper troposphere, which evolves to affect the monsoon onset convection by changing the upper divergence-pumping effect. In the lower troposphere, ENSO induces an anomalous zonal gradient of sea surface temperature (SST) over the Indian-western Pacific Ocean to alter the barotropic instability which further affects the formation of BOB monsoon onset convection. During the Indian summer monsoon onset, the anomalous convection over northeastern BOB and Indochina Peninsula in late May act to change the SAH position and its relevant upper divergence-pumping over the Arabian Sea (AS). Meanwhile, the Indian monsoon onset convection is also modulated by the ENSO-induced changes in intensity of the inertial instability and the forced convection over the AS, which are related to an ENSO-induced anomalous cross-equatorial SST gradient and zonally asymmetric meridional gradient of sea level pressure, and an anomalous westerly over the central AS in the lower troposphere. Results demonstrate that during the BOB and India monsoon onset, the influences of ENSO on the upper circulation are similar, but are distinctly different on the lower-level circulation.

Keywords South Asian summer monsoon onset · ENSO · South Asian high · Inertial instability · Forced convection

1 Introduction

As one of the most remarkable signals of seasonal transition from winter to summer in the Northern Hemisphere, the onset process of the South Asian Summer Monsoon (SASM), including the summer monsoon over the Bay of Bengal (BOB) and over India, is closely related to the occurrence of flood and drought disasters in China (Tao and Chen 1987; Chen et al. 1991; Liu and Ding 2008). The SASM onset date exhibits large interannual variability, which could be attributed to both internal processes and external forcing of the atmosphere. Although the internal atmospheric processes, i.e., the low frequency variations of atmospheric circulation, are less predictable, external forcing can facilitate better predictability of the SASM onset date (Goswami 1998). Generally, external forcing comes mainly from the slowly varying boundary, including ocean and land surfaces. Sea surface temperature (SST) has been identified as one of the major factors impacting the SASM (Chao and Chen 2001). Previous studies have pointed out that the SST anomalies in the tropical central eastern Pacific as one component of the El Niño–Southern Oscillation (ENSO) events are significantly correlated with the onset dates of summer monsoon over the BOB (Mao and Wu 2007) and India (Joseph et al. 1994; Ju and Slingo 1995). Specifically, following warm ENSO events, when warm SST anomalies appear in the tropical central eastern Pacific, the monsoon onset is postponed over the whole

B. Liu · G. Wu · R. Ren (✉)
State Key Laboratory of Atmospheric Sciences and Geophysical Fluid Dynamics (LASG), Institute of Atmospheric Physics, Chinese Academy of Sciences, Beijing 100029, China
e-mail: rrc@lasg.iap.ac.cn

SASM region; while the SASM onset is advanced following cold ENSO events, when cold SST anomalies take place in the tropical central eastern Pacific.

The processes through which ENSO influences the SASM circulation can be summarized as follows. First, ENSO can modulate the onset time and intensity of SASM by regulating the SST anomalies in other tropical oceans outside the tropical central eastern Pacific via the "atmospheric bridge". For example, winter ENSO has been found to modify the SST anomalies 4 months later in the northern Indian Ocean (Klein et al. 1999; Alexander et al. 2002; Lau and Nath 2003). The land–sea thermal contrast, air–sea interactions, and thus the summer monsoon onset process are changed in the SASM region (Lau and Nath 2012). Second, an anomalous Walker cell links the eastern pacific ENSO to the large-scale Asian monsoon circulation (Webster and Yang 1992; Wu and Meng 1998; Meng and Wu 2000). Ju and Slingo (1995) reported that during El Niño events, the tropical convection over Indonesia and western Pacific in boreal spring is suppressed due to the anomalous subsidence of Walker circulation, which is followed by delayed onset of SASM. Numerical simulations also confirm that ENSO signals can alter the meridional position of the ITCZ over the maritime continent to affect the SASM onset and its intensity (Soman and Slingo 1997). In addition, some studies have shown that ENSO can exert an impact on the thermal conditions of the Eurasian continent before the monsoon season, and the anomalous land surface conditions can in turn affect the following onset of the monsoon (Yasunari and Seki 1992; Meehl 1994). This "indirect effect" of ENSO-related SST on the SASM has also been clearly depicted by numerical experiments with GCMs (Yang and Lau 1998; Yang et al. 2004).

Despite significant advances in our understanding of the ENSO–monsoon relationship on the interannual timescale in recent years, there are still some aspects that are not quite clear. Most previous studies mainly focus on the ENSO impact on the monthly-mean background flow (e.g., Ju and Slingo 1995; Mao and Wu 2007), with less attention on synoptic processes and the related dynamical mechanisms during the onset period of SASM. Although there have been some studies concerning the effects of ENSO on either the upper- or lower-level tropospheric circulation over the SASM region in boreal summer (Kawamura 1998; Miyakoda et al. 2003), the ENSO effects on the vertical coupling between upper- and lower-atmospheric circulation systems during the SASM onset stage remain indeterminate.

The South Asian High (SAH) is the most important system in the upper troposphere over the Asian summer monsoon region in boreal summer (Mason and Anderson 1958; He et al. 2006); its evolution and the associated vertical coupling between upper and lower circulation are critical for the onset process of BOB and Indian summer monsoon (Liu et al. 2013; Zhang et al. 2014; Wu and Liu 2014). In the lower troposphere, Mao and Wu (2011) emphasized the importance of barotropic instability for the formation of Tropical Cyclone Nargis over the southeastern BOB during the summer monsoon onset in 2008. Also, the development of inertial instability and forced convection produced by the cross-equatorial pressure gradient and its zonal asymmetric distribution in the lower troposphere over the Arabian Sea (AS) have been verified to determine the generation of monsoon convection off the southwestern Indian Peninsula during the onset period of Indian summer monsoon (Wu and Liu 2014). These results suggest that the evolution of the lower level circulation during the onset stage of BOB summer monsoon may be different from that during the Indian summer monsoon. The tropical SASM onset starts over the eastern BOB (Wu and Zhang 1998; Yang et al. 2012) and ends over the India (Wang and Lin 2002; Liu et al. 2014), through which most of the ENSO events can persist (Du et al. 2009). It is then relevant to examine the differences in the onset processes of both the BOB and Indian summer monsoon between warm and cold ENSO events, which will further advance our understanding of the effects of ENSO on SASM onset.

In the current study, through a parallel comparison of the ENSO-induced circulations during the onset stage between the BOB and the Indian summer monsoon, we attempt to demonstrate how the ENSO can affect the SASM onset process by modulating the vertical coupling of circulation between the upper and lower troposphere. The remainder of the paper is organized as follows. Section 2 introduces the data and methods applied. The ENSO-related anomalies of the background circulation are discussed in Sect. 3. Sections 4 and 5 demonstrate the influences of ENSO on the onset process of the BOB and Indian summer monsoon, respectively. Finally, discussion and conclusions are presented in Sect. 6.

2 Data and methodology

The variables with a horizontal resolution of 2.5° × 2.5°, including 3-D wind fields, air temperature and specific humidity on standard isobaric surfaces, as well as the skin temperature, from the NCEP-DOE Reanalysis II data (Kanamitsu et al. 2002) during 1979–2010 are used to describe the SASM onset process. The NOAA Outgoing Longwave Radiation (OLR, Liebmann and Smith 1996) with the same horizontal resolution and same period is used as a proxy for SASM convection in the tropics. The SST and sea surface wind data are from the NOAA's high-resolution Blended Analysis of Daily SST and Blended Sea Winds datasets, respectively, with a horizontal resolution of 0.25° × 0.25°

from 1980 to 2010 (Reynolds et al. 2002; Zhang et al. 2006). The subsurface seawater temperature in the ocean is from the NCEP Global Ocean Data Assimilation System with a horizontal resolution of 1.0° × 1.0° and a vertical resolution of 40 layers from 1980 to 2010 (Behringer and Xue 2004). All the data are downloaded from the website at http://www.esrl.noaa.gov/psd/, which is provided by the NOAA/OAR/ESRL PSD, Boulder, Colorado, USA.

For comparing the onset processes of the SASM between warm and cold phases of ENSO events, it is crucial to properly define the monsoon onset dates and ENSO events. Given that the change from a southward tilting to a northward tilting of the ridge surface of the subtropical anticyclone effectively marks the seasonal transition from winter to summer, which is known to be intimately associated with the transition of the meridional temperature gradient (MTG) from negative to positive in the mid-upper troposphere (Mao et al. 2004), the reversal of the MTG is used here to identify the onset dates of summer monsoon over the BOB (Mao and Wu 2007) and India (Webster et al. 1998; Mao 2001). Note that the ridge surface always tilts toward the warmer region with increasing height, and the onset date is the time when this tilt becomes vertically perpendicular (i.e., $\partial T/\partial y = 0$). Accordingly, the onset dates of the BOB and Indian summer monsoon are defined as the dates when the following conditions are satisfied: (1) the area-averaged upper tropospheric (200–500 hPa) MTG over the eastern BOB (5°–15°N, 90°–100°E) or India (10°–20°N, 60°–85°E) changes from negative to positive; (2) the MTG remains positive for more than 10 days. To guarantee the reliability of the MTG-defined onset dates, we verified that the onset time series is highly correlated with those based on other criteria, including the area-averaged 850-hPa zonal wind and OLR respectively reaching their threshold values of 0 m s^{-1} and 230 W m^{-2}, which implicates the establishment of prevailing lower-level westerlies and deep convection over the monsoon region, respectively.

The ENSO events are defined according to the Oceanic Niño Index (ONI), which is the de-facto standard used by NOAA CPC for identifying warm (El Niño) and cold ENSO (La Niña) events. The index is the 3-month running mean SST anomaly for the Niño 3.4 region (i.e., 5°N–5°S, 120°–170°W). A warm (cold) ENSO event is defined when the Niño 3.4 anomaly is equal or above (below) +0.5 °C (−0.5 °C) for five consecutive months. Figure 1 shows the year-by-year onset dates of BOB and Indian summer monsoon (Fig. 1a, b), and the seasonal evolutions of their correlations with Niño 3.4 index (Fig. 1c). It can be seen that the onset times of both BOB and Indian summer monsoon are in general positively correlated with Niño 3.4 index from winter to the following spring, indicating that the monsoon onsets tend to be advanced following cold ENSO but postponed following warm ENSO, as also

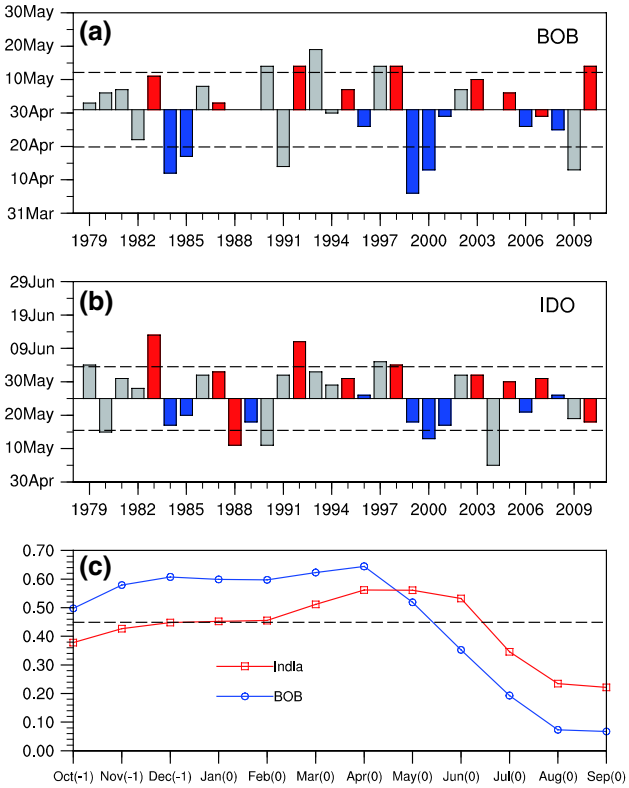

Fig. 1 Onset dates of **a** BOB and **b** Indian summer monsoon. *Red* and *blue bars* indicate years following warm and cold ENSO, respectively, **c** Correlation coefficient between Niño3.4 SST in different months and the onset date of BOB (*blue line* with *circles*) and Indian (*red line* with *squares*) summer monsoon. The *dashed lines* in (**a**) and (**b**) mark the unit standard deviation of the onset dates, and the *dashed line* in (**c**) denotes the 99 % confidence level of the correlations. The numbers "−1" and "0" in brackets on the abscissa denote the previous and current year of the summer monsoon onset, respectively

reported by other authors (e.g., Joseph et al. 1994; Mao and Wu 2007). Figure 1a, b shows that the climatology onset date of BOB and Indian summer monsoon is 1 and 25 May, respectively, whereas the BOB (Indian) summer monsoon builds up on 9 May (4 Jun) in warm ENSO years and on 19 Apr (17 May) in cold ENSO years. Although ENSO events are mature in boreal winter, the lead–lag correlation between the onset time and the Niño3.4 SST anomaly reveals that the strongest correlation between ENSO and the onset time of BOB and Indian summer monsoon is in April and May, respectively, about 3–4 months after the ENSO peak phase (Fig. 1c). Therefore, the composites of ENSO-related circulation anomalies in April and May are adopted to investigate the effect of ENSO on the onset process of the BOB and Indian summer monsoon, respectively. Before the composite analysis, we noticed that the warm ENSO event in 2006–2007 is not followed by a postponed onset of BOB summer monsoon, and the

warm ENSO events in 1987–1988 and 2009–2010 are even followed by an advanced Indian summer monsoon onset; The Indian summer monsoon onset is also delayed in 1996 and 2008, when cold ENSO events occur in the previous winter. Case-by-case analysis indicates that the reason for these exceptions is the faster-than-normal decay of ENSO events in these years (figures not shown). On average, ENSO events can persist from the previous winter to the following early summer. However, the warm ENSO events in 1987–1988, 2006–2007, and 2009–2010 are damped before April in early spring, also as the cold ENSO events in 1995–1996 and 2007–2008. The much earlier termination of these ENSO events limits their remote effects on Indo-Pacific oceans within spring months (Li et al. 2012) and their influences on the SASM onset processes in early summer. Though our correlation analysis still indicates a statistically significant relationship between the SASM onset and the Niño3.4 index in the preceding winter, even when these ENSO cases are included, we have excluded these short-lived ENSO events in our composite analysis to demonstrate the ENSO effects on the SASM onset more clearly. After excluding those short-duration ENSO events, there are in total, seven warm events starting in the winters of 1982, 1986, 1991, 1994, 1997, 2002 and 2004, and seven cold events starting in the winters of 1983, 1984, 1988, 1998, 1999, 2000 and 2005. A "warm composite" and a "cold composite" are then obtained, and the dynamic and thermodynamic roles of ENSO in both the BOB and the Indian monsoon onset are investigated through a parallel comparison between these two composites.

3 Anomalies of spring background circulation associated with ENSO

Since the onset process of the BOB and Indian summer monsoon occurs in late April and late May, respectively, we first investigate the different background circulations in these 2 months in relation to ENSO events. Previous studies have suggested that the duration of warm and cold ENSO events is asymmetric (e.g., Okumura and Deser 2010), here in Fig. 2 we firstly analyze the warm and cold composites to check whether such asymmetry could influence the SASM onset process. In April, the composed SST anomalies are basically symmetric between the warm and cold ENSO events, so as the anomalous sea surface wind and 200-hPa velocity potential (Fig. 2a–d). The warm (cold) SST anomalies are located in the tropical central eastern Pacific, the equatorial and the southwestern Indian Ocean in the warm (cold) ENSO composites. Negative (positive) anomalies of equatorial zonal SST gradient in the Indian–western Pacific Ocean correspond to the surface easterly (westerly) anomalies along the equator. In the equatorial eastern Pacific Ocean in May, however, although the cold SSTA persists after cold ENSO, the warm SSTA after warm ENSO tends to dramatically weaken. Such asymmetries between El Niño and La Niña were also reported in Okumura and Deser (2010). This asymmetry also exists in the equatorial eastern Indian Ocean where the warm SSTA presents in the warm ENSO composite in association with the enhanced onshore current off the Sumatra (Fig. 2e); while in the cold ENSO composite, cold SSTA is located in the northern AS and associated with the stronger local anomalous surface wind (Fig. 2g). Over the western equatorial AS, however, the SSTA and the circulation are still apparently symmetric as can be seen from Fig. 2e–h: in the warm/cold ENSO composite warm/cold SSTA resides to the south of equator, which is induced by the stronger in situ anomalous surface wind (Xie 1996; Wu and Meng 1998; Klein et al. 1999; Wu et al. 2008). Consequently, the lower-layer cross-equatorial southerly over the AS is weakened/strengthened in the warm/cold composite (Fig. 2e, g), in coordination with the weakened/strengthened upper-layer cross-equatorial northerly due to the opposite geopotential anomalies straddling the equator there (Fig. 2f, h). In addition, the anomalous OLR and surface zonal wind induced by warm events are almost out-of-phase with those induced by cold events over the AS (Fig. 3). These all imply that the response of relevant SSTA, the atmospheric circulation and convection in the Asian monsoon area are generally symmetric but out-of-phase following warm and cold ENSO events.

The large-scale anomalies of background circulation in warm and cold ENSO composites are also displayed in terms of the velocity potential and divergent wind at 200 hPa. In the warm ENSO composites, associated with the warm (cold) SSTA over the tropical eastern (western) Pacific in April (Fig. 2a), evident anomalies of ascent (descent) accompanied with divergent (convergent) flow appear in the upper troposphere (Fig. 2b). The composite SST and vertical motion anomalies for the cold ENSO events exhibit a general out-of-phase structure (Fig. 2c, d). Similarly, in the lower troposphere (Fig. 3a, c), the anomalous 850-hPa easterlies (westerlies) prevail over the southern BOB in April due to the local negative (positive) zonal gradient of SST anomalies near the equator; while anomalous westerlies (easterlies) exist over the western Pacific due to the local positive (negative) zonal gradient of SST anomalies and the anomalous anticyclone (cyclone) over the western North Pacific Ocean (Zhang et al. 1999; Wang et al. 2000; Zhang and Sumi 2002) in the warm (cold) ENSO composites. Subsequently, convection over the Philippines is suppressed (enhanced) in the warm (cold) ENSO composites (Fig. 3b, d) where the anomalous zonal flow diverges (converges) in the lower troposphere (Fig. 3a, c). Meanwhile, convection over the eastern BOB and to the north of the maximum anomalous easterlies (westerlies) is also weakened (strengthened), indicating a

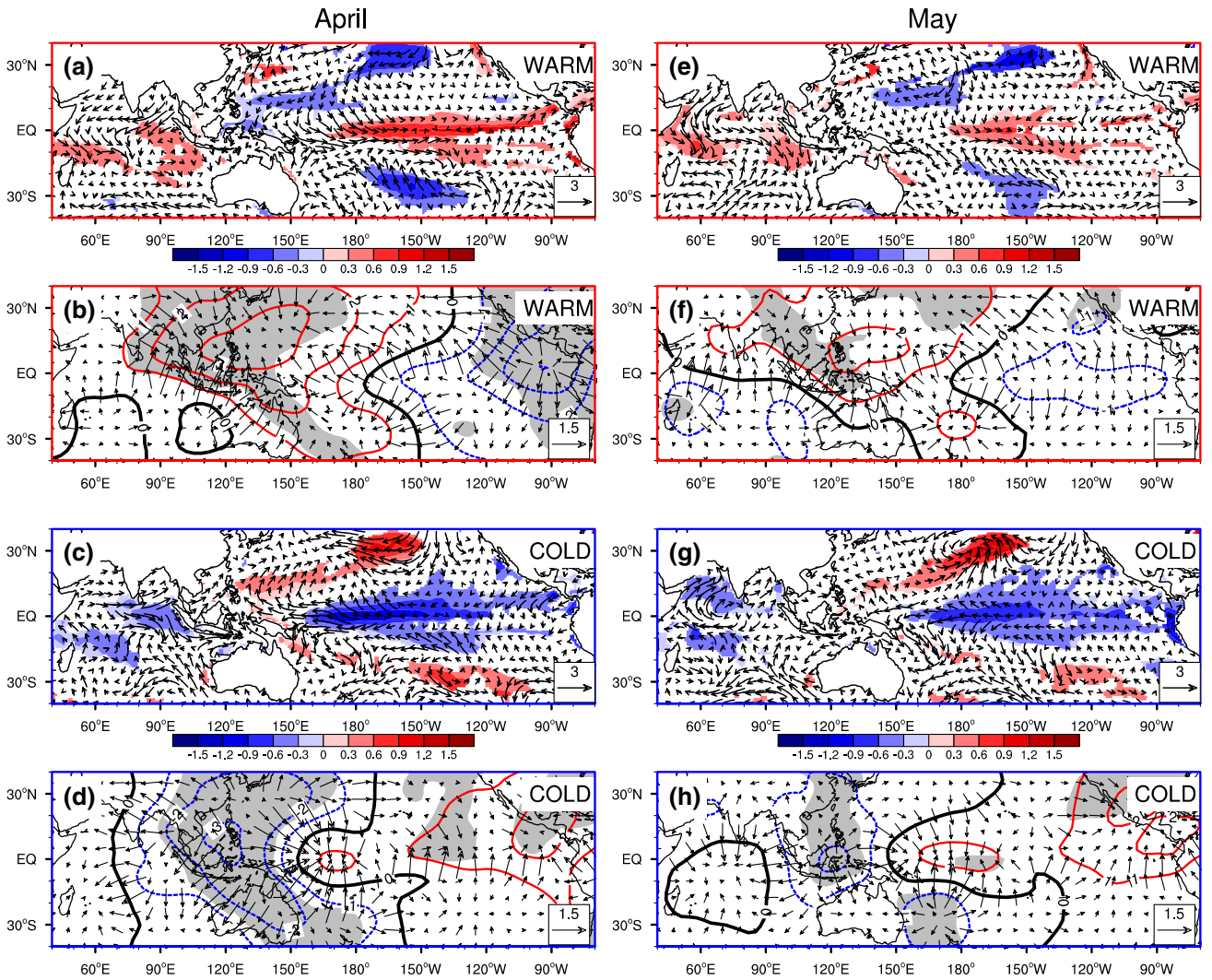

Fig. 2 Cold and warm composites of **a**, **c**, **e**, **g** SST anomaly (*shading*, °C; only values above the 90 % confidence level are plotted) and sea surface wind (*vectors*, m s^{-1}); **b**, **d**, **f**, **h** velocity potential (*contours*, 10^6 m^2 s^{-1}) and divergent wind at 200 hPa (*vectors*, m s^{-1}) in April (*left column*) and May (*right column*). *Gray shading* in (**b**, **d**, **f**, **h**) marks the 90 % confidence level of the composites. *Red* and *blue panel* frameworks represent the warm (**a**, **b**, **e**, **f**) and cold (**c**, **d**, **g**, **h**) composites, respectively

weakening (enhancing) barotropic instability over the eastern BOB and potential late (early) onset of the BOB summer monsoon following warm (cold) ENSO events.

In May, compared with in April the anomalies of both descent (ascent) over the western Pacific and ascent (descent) over the eastern Pacific are weakened in the warm (cold) ENSO composites, respectively (Fig. 2f, h). The zonal gradient of SST anomalies is thus attenuated to dampen the anomalous 850-hPa equatorial zonal flows over the BOB and Central Pacific (Fig. 3e, g) and the resultant divergence (convergence) over the western Pacific as represented by the positive (negative) OLR anomalies (Fig. 3f, h). On the other hand, intensified asymmetric circulations develop over the AS: corresponding to the weakened (strengthened) cross-equatorial southerly there (Fig. 2e, g), anomalous easterlies (westerlies) and westerlies (easterlies) straddle the equator (Fig. 3e, g), consistent with the enhanced warming (cooling) in the southwestern Indian Ocean and the resultant weaker (stronger) cross-equatorial gradient of SST anomalies in the western AS (Fig. 2e, g) in the warm (cold) ENSO composites. Meanwhile, the convection is suppressed (enhanced) over the eastern AS in the warm (cold) ENSO composites (Fig. 3f, h), indicating a late (early) onset of Indian summer monsoon under the influence of warm (cold) ENSO events. The association between the anomalous cross-equatorial SST gradient in the western AS and the convection anomaly over the eastern AS in Northern Hemisphere will be further examined in Sect. 5.3 based on the theory of inertial and forced unstable convection development (Tomas et al. 1999; Wu and Liu 2014).

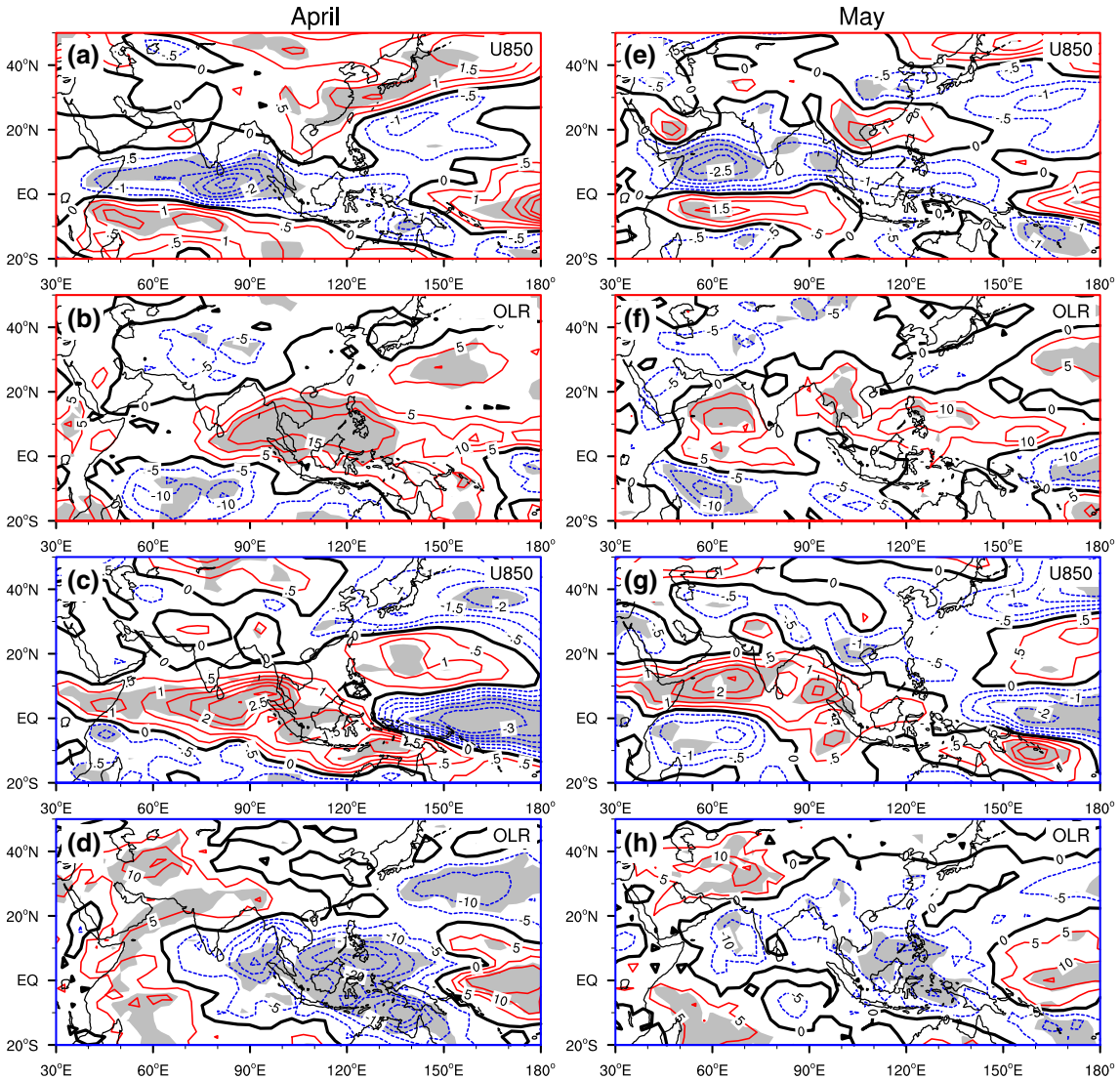

Fig. 3 Cold and warm composites of the **a**, **c**, **e**, **g** zonal wind anomaly at 850 hPa (m s^{-1}), and **b**, **d**, **f**, **h** OLR anomaly (W m^{-2}) in April (*left column*) and May (*right column*). *Gray shading* indicates the 90 % confidence level of the composites. *Red* and *blue* panel frameworks represent the warm (**a**, **b**, **e**, **f**) and cold (**c**, **d**, **g**, **h**) composites, respectively

The results presented above demonstrate that ENSO events can modulate the onset time of summer monsoon over the BOB and India by modifying the SST and the large-scale circulation over the SASM region. Generally, the response of the relevant atmospheric circulation and convection from April to May is symmetric but out-of-phase following warm and cold ENSO events. Moreover, results from the composite analyses based on the onset time of BOB and Indian summer monsoon (figures not shown) also prove that the onset date of BOB summer monsoon is closely related to the equatorial zonal gradient of SST anomalies over the BOB in April, while the Indian summer monsoon onset date is intimately associated with the meridional gradient of SST anomalies over the western AS in May. More importantly, The ENSO-induced SST anomalies in the BOB and AS are both generally symmetric between warm and cold ENSO events. Thus in the following analysis, the cold-minus-warm composites are specifically displayed to highlight the ENSO effects on the SASM onset.

4 ENSO influences on the BOB summer monsoon onset

4.1 Upper tropospheric circulations

To demonstrate the synoptic-scale characteristics of the BOB onset process, pentad-mean composite differences of variables between cold and warm ENSO events in the

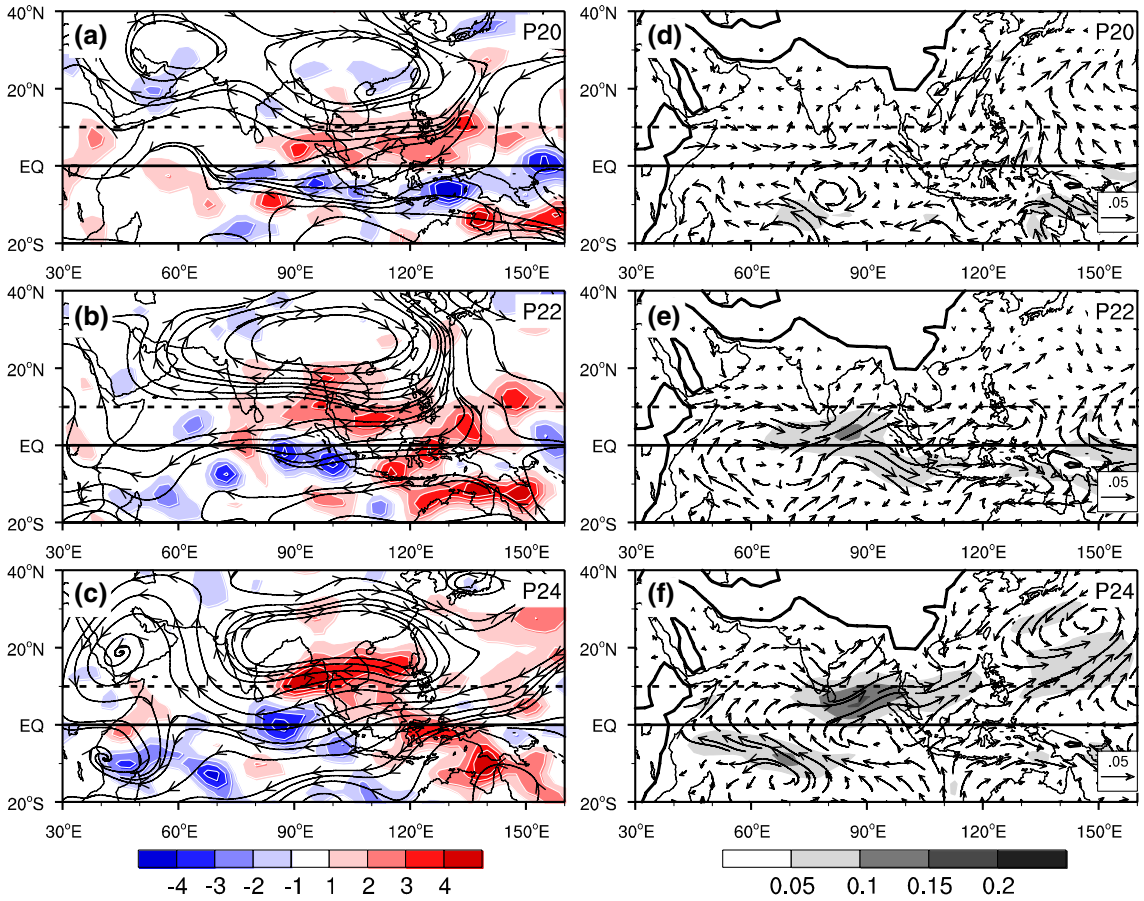

Fig. 4 Cold-minus-warm composites of the **a**–**c** 200-hPa streamline and 500-hPa diabatic heating (*shading*, K day^{-1}), and **d**–**f** 925-hPa humidity transport (*vectors*, kg m kg^{-1} s^{-1}) and its magnitude (*shading*, kg m kg^{-1} s^{-1}) during the BOB summer monsoon onset from Pentad 20 to Pentad 24. *Bold curves* in (**d**–**f**) mark the topography

upper and lower troposphere are shown in Fig. 4. The diabatic heating Q_1 used here is calculated with the scheme deduced by Yanai et al. (1973), which takes the form

$$Q_1 = C_p \left[\frac{\partial T}{\partial t} + \vec{V} \cdot \nabla_h T + \left(\frac{p}{p_0} \right)^{R/C_p} \omega \frac{\partial \theta}{\partial p} \right] \quad (1)$$

in which T, C_p and R are the air temperature, the specific heat of dry air at constant pressure and the gas constant for dry air, respectively. Following cold ENSO events in the upper troposphere, an anomalous anticyclone appears above the land to the north of the Indochina Peninsula from Pentad 20–22 before the BOB summer monsoon onset (Fig. 4a, b), presenting a Gill-type response (Gill 1980) to the anomalous diabatic heating over the southern South China Sea and Philippines (Fig. 3d) resulted from the stronger lower convergence (Fig. 3c). The most evident anomalies of diabatic heating are at Pentad 24 over the northeastern BOB, implying an earlier onset of BOB summer monsoon (Fig. 4c). Meanwhile, the anomalous anticyclone persists to the north of the stronger diabatic heating over the BOB, indicating that the SAH tends to stay to the north of its climate-mean position during the onset stage of BOB summer monsoon after cold ENSO event. Subsequently, the existing anomalous easterlies on the south of the SAH and the northeasterlies near the equator compose a stronger divergent pattern (Fig. 4c), which acts as an upper tropospheric pumping over the eastern BOB and thus favors an earlier onset of BOB summer monsoon.

4.2 Lower-tropospheric circulations

In the lower troposphere, the positive zonal gradient of SST anomalies in the cold-minus-warm composite produces anomalous westerlies over the southern BOB in conjunction with the anomalous cyclone over the western North Pacific triggered by the cold SST anomaly in the tropical central–eastern Pacific (Figs. 2c and 3c), it helps to bring more moisture into the BOB during the BOB summer monsoon onset (Fig. 4d, e), especially at Pentad 24 (Fig. 4f) when the westerlies are strengthened to the south of 10°N over the BOB (Fig. 5a). Moreover, the anomalous

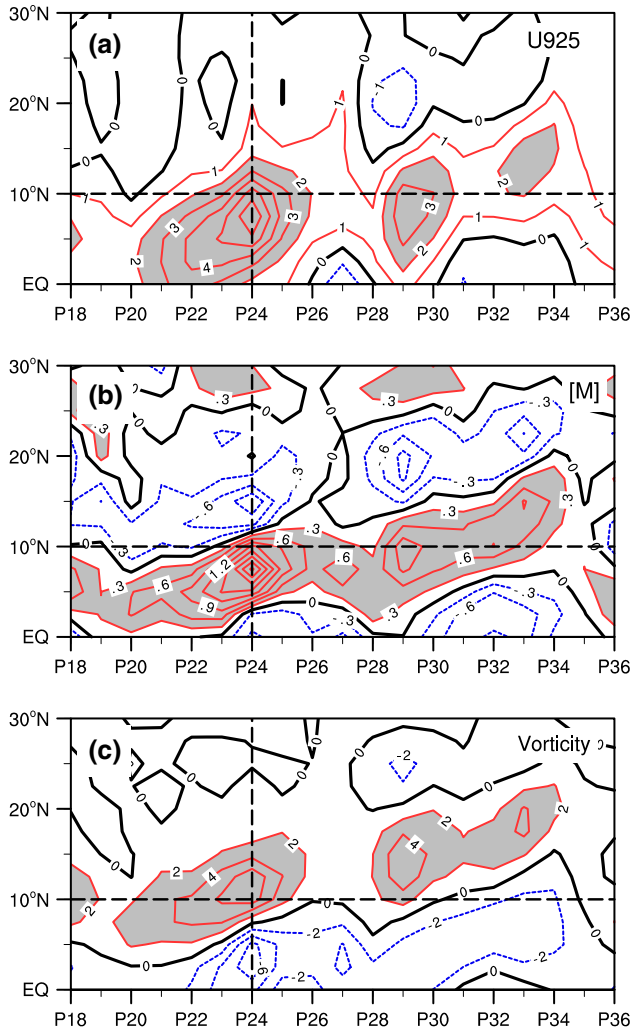

Fig. 5 Temporal evolution of cold-minus-warm composites of **a** zonal wind (m s^{-1}), **b** meridional gradient of absolute vorticity [*M*] (10^{-11} m^{-1} s^{-1}) and **c** relative vorticity (10^{-6} s^{-1}) averaged from 70°E to 110°E at 925 hPa. Values of anomalous zonal wind, meridional gradient of absolute vorticity and relative vorticity >2 m s^{-1}, 0.3 × 10^{-11} m^{-1} s^{-1}, and 2 × 10^{-6} s^{-1}, respectively, are shaded in *light gray*

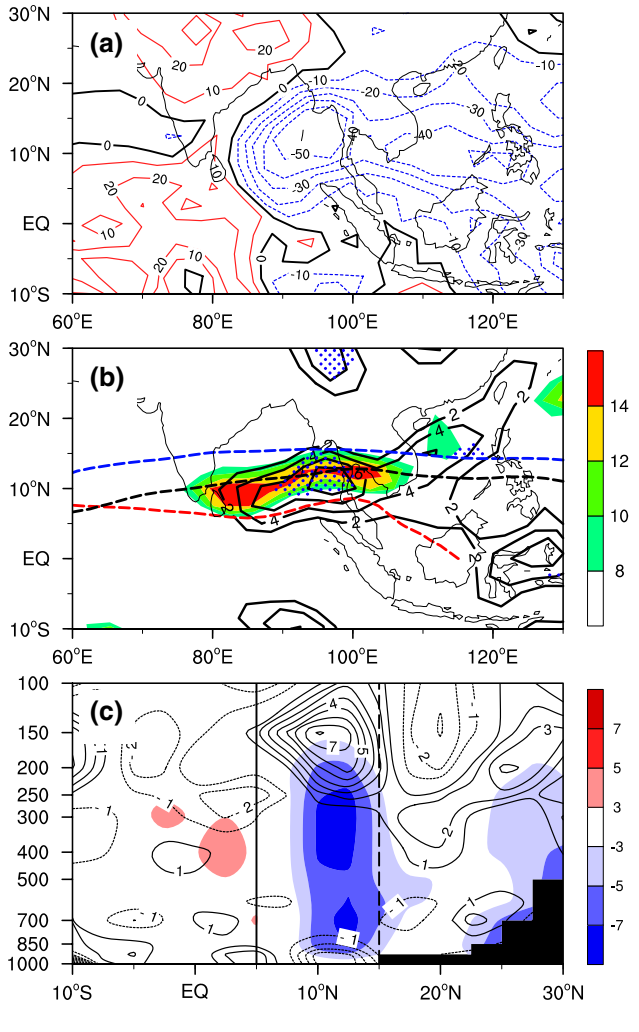

Fig. 6 Cold-minus-warm composites at Pentad 24 of the horizontal distribution of **a** OLR (W m^{-2}), **b** 850-hPa relative vorticity (*shading*, 10^{-6} s^{-1}), 150-hPa divergence (*solid contours*, 10^{-6} s^{-1}) and 400-hPa ascent (>6 × 10^{-2} pa s^{-1}, *stippled*), *red* and *blue dashed lines* denote the SAH ridgeline at 150 hPa after warm and cold ENSO, respectively, *black dashed line* is for the climatological position of 150-hPa SAH ridgeline; and **c** 90°–100°E averaged pressure–latitude cross-section of vertical motion (*shading*, 10^{-2} pa s^{-1}) and divergence (*contour*, 10^{-6} s^{-1}) over the BOB

westerlies can strengthen the negative meridional shear of zonal wind to enhance the barotropic instability over the northeastern BOB. As suggested by Krishnamurti et al. (1981), the barotropic instability of zonal flow with horizontal shear can be measured by the meridional gradient of absolute vorticity which is expressed as

$$[M] = -\frac{\partial^2}{\partial y^2}[u] + \beta, \tag{2}$$

where M represents the meridional gradient of absolute vorticity, u is the zonal wind, β denotes the meridional gradient of the Coriolis parameter, and the square brackets denote zonal mean. Following Mao and Wu (2011), the zonal-mean flow averaged between 70°E and 110°E is chosen to represent the basic flow over the BOB. The temporal evolution of [*M*] is presented in Fig. 5b, showing the existence of zero contours of [*M*] and barotropic unstable circulation over the southern BOB. Meanwhile, an abnormal cyclonic vorticity is formed to the north of the anomalous westerlies (Fig. 5c). This implies that the anomalous westerlies due to the zonal gradient of SST anomalies facilitate the formation of monsoon onset vortex over the northern BOB by generating the barotropic unstable circulation in the lower troposphere in the onset stage of BOB summer monsoon.

4.3 Vertical coupling of circulations

To demonstrate the features of vertical coupling between the upper and lower circulations during the BOB summer monsoon onset, Fig. 6 shows the cold-minus-warm composite distributions over the BOB at Pentad 24 of OLR (Fig. 6a), 850-hPa relative vorticity (shading in Fig. 6b), 150-hPa divergence (solid contours in Fig. 6b), 400-hPa ascent (stippling in Fig. 6b), as well as the pressure–latitude cross-section of vertical motion (shading in Fig. 6c) and divergence (contours in Fig. 6c). Following the cold ENSO events, convection is first enhanced near the southern South China Sea and Philippines in late April (Fig. 3d) because of the lower-tropospheric anomalous convergence induced by the equatorial zonal gradient of SST anomalies in the Indian–Pacific Ocean (Figs. 3c, 4f). Then, at Pentad 24, an anomalous anticyclone to the north of Indochina Peninsula is stimulated by the stronger convection, leading the SAH to the north of its climate-mean position near 10°N (Fig. 4c). As a result, a stronger upper divergent streamline field develops just over the northeastern BOB (Fig. 4c) accompanied by anomalous divergence and ascent in the middle troposphere (Fig. 6b). The superposition of upper divergence and mid-level ascent manifests the anomalous divergence-pumping effect on the formation of monsoon convection over the BOB (Fig. 6c). In the lower troposphere, the anomalous westerlies over the southern BOB not only enhance moisture transport to the eastern BOB, but also increase the barotropic instability of basic flow ($[M] > 0$) to encourage the formation of monsoon vortex (Fig. 5c). However, above the low-level center of anomalous vorticity near Sri Lanka, there is no upper-level anomalous divergence superposed. Consequently, the upper and lower circulation becomes uncoupled there, and no in situ ascent anomaly develops. All these signify the importance of the earlier upper- and lower- level coupling for the BOB monsoon onset forced by the cold ENSO events.

5 Impacts of ENSO on the Indian summer monsoon onset

5.1 Upper-tropospheric circulations

Prior to the Indian summer monsoon onset land–sea thermal contrast over the BOB is enhanced with an evident cooling above the BOB from Pentad 28–29 (Fig. 7a, b) and a further strengthened warming over land to the north of BOB at Pentad 30 following cold ENSO events (Fig. 7c). Hence the BOB monsoon convection is enhanced tremendously over the northeastern BOB and the Indochina Peninsula before the Indian summer monsoon onset (Fig. 8a, b). Consequently, an anomalous anticyclone in the upper troposphere develops over the Iranian Plateau to the north of the AS manifesting itself as a Gill-type response to the stronger BOB monsoon convection (Fig. 8a–c). This anomalous anticyclone indicates a northwestward expansion of the SAH following cold ENSO events. Subsequently, the southerlies on the west of this anomalous anticyclone and the northeasterlies near the equator compose an anomalous "trumpet-shape" streamline, and further intensify the upper divergence-pumping over the AS at Pentad 30 (Figs. 8c and 9a), promoting the generation of earlier Indian monsoon convection (Fig. 9b).

5.2 Lower-tropospheric circulation

Below the aforementioned upper anomalous anticyclone, there exist descent anomalies over the Iranian Plateau to suppress the local convection (Fig. 9b). The descent anomalies, which act as the sinking branch of Rossby-wave responses to the intensified monsoon convection over the BOB, then strengthen the MTG by warming the air column over land to the north of AS (Fig. 7d–f). The resultant decreased rainfall over land also acts to raise the local land surface temperature and enhances the land–sea thermal contrast (Fig. 9c), and thus can intensify the westerly across the AS after cold ENSO events (Fig. 8d–f). Such a lower-tropospheric westerly anomaly together with the enhanced cross-equatorial flow transport anomalous moisture into the AS at Pentad 30 (Fig. 8f), followed by the enhanced convection off the southwestern Indian Peninsula, implying an early onset of Indian summer monsoon ensuing cold ENSO (Fig. 9b).

It is important to note that the presence of cross-equatorial flow over the AS during the Indian monsoon onset makes it distinct from the BOB summer monsoon onset. Actually, such a difference can be ascribed to the different features of SST anomaly between April and May. Compared with the evident zonal gradient of SST anomalies over the BOB in April (Fig. 2a, c), the cross-equatorial gradient of SST anomalies over the western AS is much stronger in May (Fig. 2e, g). Such difference is attributed to the distinct thermocline depth between the southwestern and northern Indian Ocean (Xie et al. 2002). Figure 10 elucidates that the stronger cross-equatorial SST gradient over the AS starts with the SST cooling in the southwestern Indian Ocean ascribed to the oceanic dynamic process in May following cold ENSO events. Since the thermocline is shallow in the southwestern Indian Ocean, the upwelling of cold water induced by the surface easterly anomalies can affect local SST after cold ENSO events (Figs. 2g, 10a, b). When the cold water reaches the near-equatorial sea surface in the southern hemisphere, the cold SST anomalies are formed to produce a stronger cross-equatorial SST gradient at Pentad 28 (Fig. 10c). Afterwards the stronger southwesterly to the

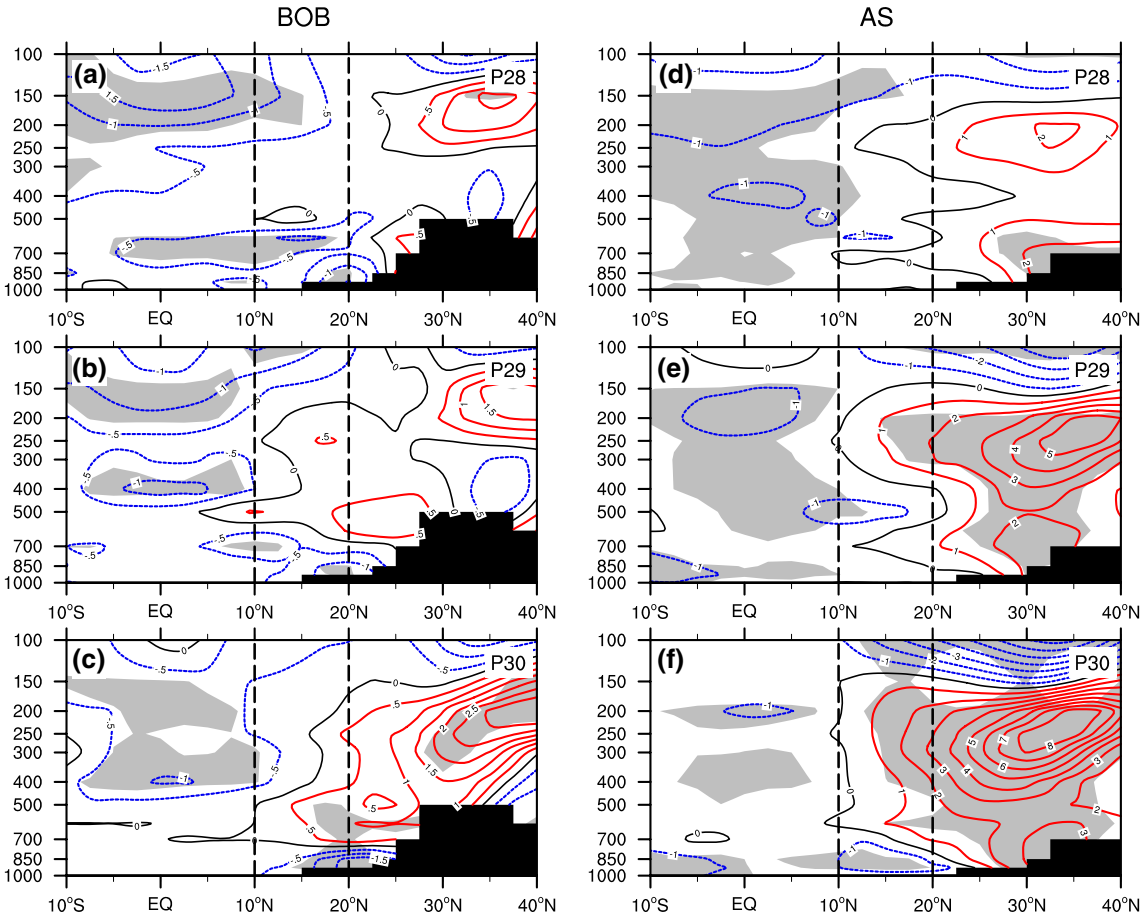

Fig. 7 Pressure–latitudinal crossing section of cold-minus-warm composites of air temperature (*contours*, K) averaged over **a**–**c** the BOB (90°–100°E) and **d**–**f** the Arabian Sea (60°–75°E) from Pentad 28–30, respectively. *Gray shading* denotes the 90 % confidence level of the composites. *Dark shading* is for the topography

north of the equator will decrease the SST in the AS with deep thermocline by the wind-evaporation-SST feedback (Figs. 8e, f and 10d–f).

The evolutions of the cross-equatorial gradients of SST and 925-hPa geopotential height from Pentad 18–36 following cold and warm ENSO are presented in Fig. 11a, b, respectively. The climatological mean is also displayed for comparison. The cross-equatorial gradient is defined as the difference of area-averaged values between (0–15°N, 50°–70°E) and (15°S–0, 50°–70°E), as marked in (c) by thin-lined boxes. The positive cross-equatorial SST gradient before Pentad 30 is stronger following cold ENSO than following warm ENSO (Fig. 11a). This is in accordance with the stronger negative meridional gradient of lower-level pressure following cold ENSO (Fig. 11b). After the establishment of monsoon convection, the cross-equatorial gradient of SST over the AS decreases quickly following both cold and warm ENSO. However, the monsoon depression develops and further amplifies the negative meridional gradient of lower-level pressure after monsoon onset. The distinct cross-equatorial SST and pressure meridional gradient can generate significant changes of the atmospheric circulation according to the theory of inertial instability (Tomas et al. 1999) and forced convection (Wu and Liu 2014).

5.3 Inertial instability and forced convection

As emphasized in Wu and Liu (2014), by generating inertial instability and forced convection, the cross-equatorial gradient of lower -level pressure is important for the onset process of Indian summer monsoon. According to Tomas et al. (1999) and Wu and Liu (2014), the equation controlling the atmospheric meridional movement in the boundary layer can be expressed as

$$\frac{D^2v}{Dt} + \lambda^2 v = f\left(\frac{\partial u_g}{\partial t} + u\frac{\partial u_g}{\partial x}\right) + Kf(2u - u_g), \tag{3}$$

where $\lambda^2 = f\left(f - \frac{\partial u_g}{\partial y}\right) - K^2$ and $u_g = -\frac{1}{f}\frac{\partial \phi}{\partial y}$ are the inertial instability criteria and the zonal component of

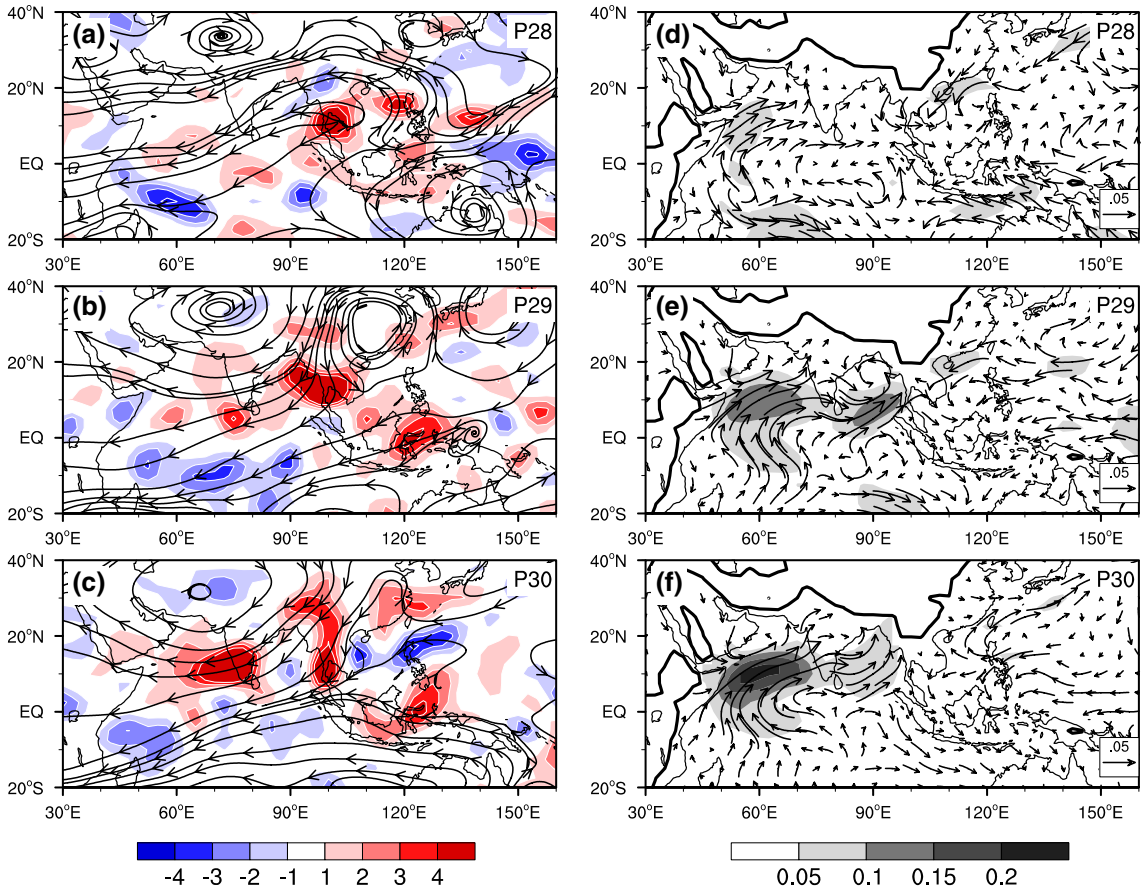

Fig. 8 Cold-minus-warm composites of the **a**–**c** 150-hPa streamline and 500-hPa diabatic heating (*shading*, K day^{-1}), and **d**–**f** 925-hPa humidity transport (*vectors*, kg m kg^{-1} s^{-1}) and its magnitude (*shading*, kg m kg^{-1} s^{-1}) during the Indian summer monsoon onset from Pentad 28 to Pentad 30. *Bold curves* in (**d**–**f**) mark the topography

geostrophic wind, respectively; and u, v, f, ϕ and K are the zonal wind, meridional wind, Coriolis parameter, geopotential and frictional coefficient, respectively. Here, the meridional component of geostrophic wind is neglected because of its smaller scale than that of the zonal component. Inertial instability occurs when $\lambda^2 < 0$ is satisfied, and its strength can be measured by the northward shift of the contour of zero absolute vorticity ($\eta = 0$, Tomas and Webster 1997). Forced convection associated with meridional acceleration of v develops when the meridional pressure gradient increases downstream of a westerly flow. Its effect can be represented by the meridional ageostrophic wind response (v_1^*) and its convergence (dv_1^*/dy), which is ascribed to the meridional pressure gradient and its zonal asymmetric distribution in the planet boundary layer (Wu and Liu 2014):

$$v_1^* \approx -\frac{1}{\lambda^2}\left(u\frac{\partial}{\partial x}\right)\left(\frac{\partial \phi}{\partial y}\right). \quad (4)$$

For the strength of inertial instability and forced convection, the average meridional position of the $\eta = 0$ contour and the forced meridional wind (v_1^*) in the northern hemisphere are significantly distinct at Pentad 30 between cold and warm ENSO (Fig. 11c). After cold ENSO, the $\eta = 0$ contour is pushed more northward over the AS, and the v_1^* at Pentad 30 is stronger off the southwestern Indian Peninsula (Fig. 11c). This is because the meridional gradient of geopotential height at 925 hPa after cold ENSO gets intensified (Fig. 11d, e). Following Tomas and Webster (1997), the stronger meridional gradient of geopotential height pushes the $\eta = 0$ contour northward to 6°N, while the weaker meridional gradient of lower-level pressure after warm ENSO corresponds to a near-equatorial $\eta = 0$ contour (Fig. 11c). Since larger inertial instability can result in stronger westerlies to the north of the $\eta = 0$ contour via the ageostrophic process (Tomas et al. 1999), the westerlies over the central AS near 60°E are strengthened during the Indian summer monsoon onset after cold ENSO (Fig. 11f). However, the anomalous center of convection is not to the north of the anomalous westerlies. Instead, it is located to the east of the anomalous westerlies, off the southwestern Indian Peninsula (Fig. 9b) at Pentad 30. Such a

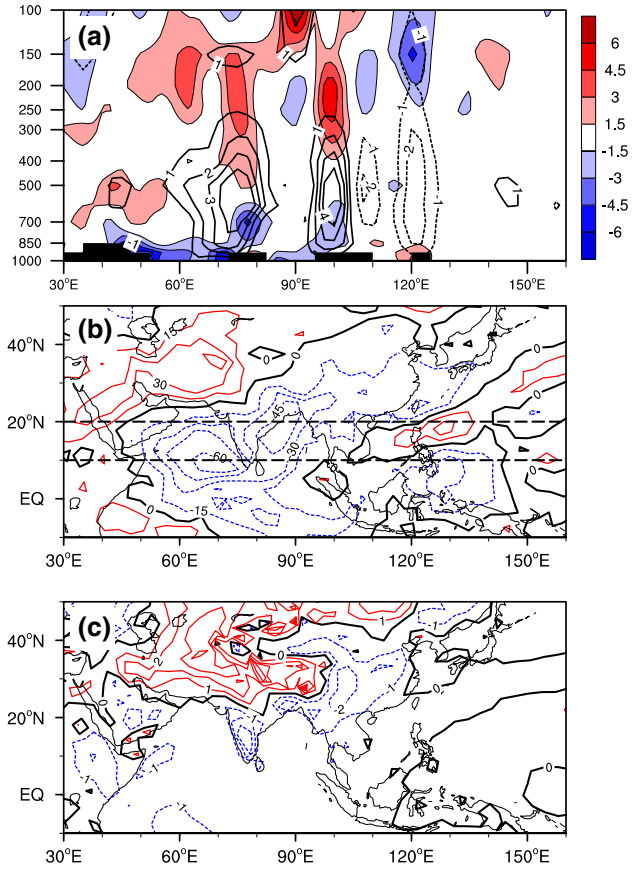

Fig. 9 Cold-minus-warm composites at Pentad 30 of **a** 10°–20°N averaged pressure–longitude cross-section of diabatic heating Q_1 (*contours*, K day^{-1}) and divergence (*shading*, 10^{-6} s^{-1}), and horizontal distribution of **b** OLR (W m^{-2}) and **c** skin temperature (K)

configuration of zonal wind and convection difference can be explained by the theory of forced convection development: the difference of forced convection is ascribed to the zonal asymmetric distribution of the meridional gradient of geopotential height (Fig. 11e) in conjunction with the anomalous westerlies (Fig. 11f), as described by Eq. (4). As shown in Fig. 11c, the ENSO-induced v_1^* anomaly is as large as its climatological value, indicating the great interannual variability of, and the significance of ENSO impact on, the onset process of Indian summer monsoon.

Figure 12 shows the OLR, v_1^*, and its meridional gradient at Pentad 30 after warm and cold ENSO. The stronger meridional pressure gradient after cold ENSO leads to northward extended stronger westerlies over the central AS (Fig. 12a) and intensified ageostrophic southerly v_1^*, resulting in an evident convergence center off the southwestern Indian Peninsula (Fig. 12b) which accelerates the onset of Indian summer monsoon after cold ENSO. On the contrary, after warm ENSO the meridional pressure gradient is too weak to engender strong westerlies over the central AS (Fig. 12c). Subsequently, the lower-level convergence associated with the much weaker v_1^* is not strong enough to develop the monsoon convection off the southwestern Indian Peninsula at Pentad 30 (Fig. 12d). Therefore, the onset time of the Indian monsoon is postponed after warm ENSO.

Results from Sects. 4 and 5 demonstrate that the vertical coupling of the upper and lower tropospheric circulation is important for the advanced/delayed onset of summer monsoon after cold/warm ENSO event over both BOB and Indian regions. However the intensities of these circulations are different in the two regions. Figure 13a presents the evolution of the anomalous upper tropospheric divergence averaged between 5°N and 20°N where the maximum divergence pumping is located during the SASM onset. During the incubation period of the advanced BOB monsoon onset before Pentad 24, strong upper-layer divergence anomalies of more than 3×10^{-6} s^{-1} develop over the eastern BOB and western Indochina Peninsular. Whereas during the incubation period of the advanced Indian monsoon onset before Pentad 30, the upper-layer divergence anomalies over the AS are relatively weaker (~2×10^{-6} s^{-1}). This implies that the ENSO-induced anomalies of the upper tropospheric pumping during BOB onset are stronger than that over the AS during the Indian monsoon onset. In addition, Fig. 13b shows the evolution of the 850-hPa vorticity averaged between 5°N and 20°N, where the maximum convection is located during the SASM onset. And the lower-layer vorticity anomalies over the BOB are about 6×10^{-6} s^{-1} before the advanced BOB monsoon onset, but it is stronger (>8×10^{-6} s^{-1}) over the AS before the advanced Indian monsoon onset, implying the significance of ENSO impact on the change of the cross-equatorial gradient of SST anomalies and the forced convection during the Indian monsoon onset.

6 Summary and discussion

Composite differences between cold and warm ENSO in circulation anomalies in the following spring indicate that cold (warm) ENSO can induce cold (warm) SST anomalies over the BOB and AS via the "atmospheric bridge", so that the meridional land–sea thermal contrast is enhanced (weakened) to advance (postpone) the SASM onset date. Composite results also show that cold (warm) ENSO events exert their influences on SASM onset mainly by inducing an earlier (later) and stronger (weaker) vertical coupling between the upper- and lower-level circulations. Moreover, it is demonstrated that the influences of ENSO on the onset process are different between the BOB and the Indian summer monsoon, especially in the lower troposphere, due to to the different features of the ENSO-induced SST anomalies between the BOB and the AS. This suggests that ENSO's

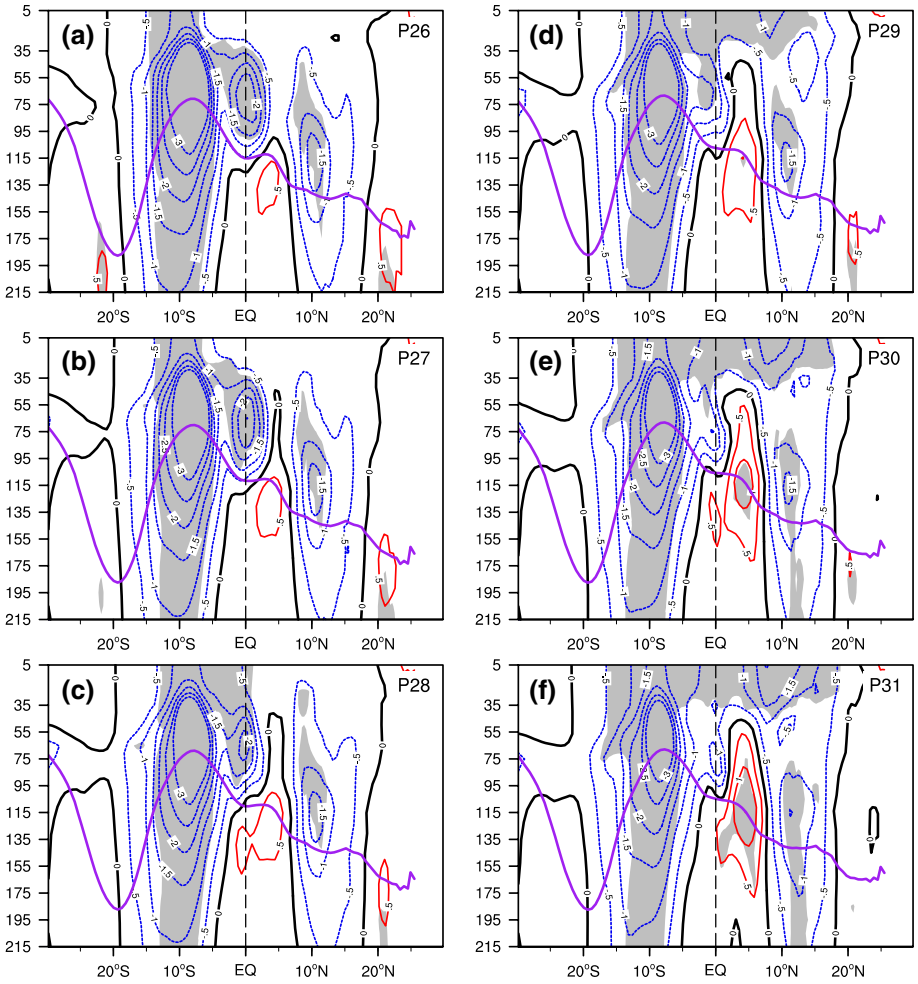

Fig. 10 Depth–latitudinal crossing section averaged between 50°E and 70°E of cold-minus-warm composites of seawater temperature anomalies (*blue* and *red contours*, °C) from Pentad 26–31. *Purple bold lines* are for the 20 °C isotherm. *Gray shading* represents the 90 % confidence level of the composites

influences on the SASM onset are largely passed by these ENSO-related SST anomalies over the Indian Ocean.

Specifically, after cold ENSO, SST anomalies are positive over the western Pacific but negative over the Indian Ocean and the central eastern Pacific, producing westerly anomalies over the southern BOB and easterly anomalies over the western Pacific. Anomalous convergence is then generated over the Philippines, yielding strengthened local convection, which in turn leads the SAH to the north of its climate-mean position over the Indochina Peninsula. Stronger pumping thus appears over the northeastern BOB because of the anomalous divergence in the upper troposphere. Meanwhile, the positive zonal gradient of SST anomalies along the equator induces the local lower-tropospheric anomalous westerlies over the southern BOB, which are conducive to the genesis of the mon soon onset vortex by increasing the barotropic instability of zonal basic flow over the northern BOB. Accordingly, both the intensified upper divergence-pumping and the enhanced lower positive vorticity facilitate an early onset of BOB summer monsoon following cold ENSO by vertically coupling between upper- and lower-level circulations.

During the onset stage of the Indian summer monsoon, although ENSO events have been damped, the ENSO-related cold SST anomalies in the BOB can persist until late May via wind–evaporation–SST (WES) feedback after cold ENSO (Xie 1996). Thus, the strengthened local land–sea thermal contrast favors stronger monsoon convection over the BOB. In the upper troposphere, the anomalous anticyclone is situated over the Iranian Plateau, acting as a Gill-type response to the condensation heating released by the stronger BOB monsoon convection. Therefore, an anomalous "trumpet-pattern" stream field forms over the AS to provide a favorable upper divergence-pumping background for the Indian summer monsoon onset. In addition, the SST anomalies in the southwestern Indian Ocean are cold in May due to the local upwelling of cold water associated with cold ENSO. Subsequently, the cross-equatorial SST gradient over the western Indian Ocean gets stronger to enhance the meridional gradient of lower-level pressure. Therefore, the inertial instability intensifies to strengthen the westerlies in the lower troposphere over the AS. When the anomalous westerlies arrive at the southwestern Indian Peninsula, the southerlies in situ are coincidentally strengthened by the zonal increase of meridional pressure

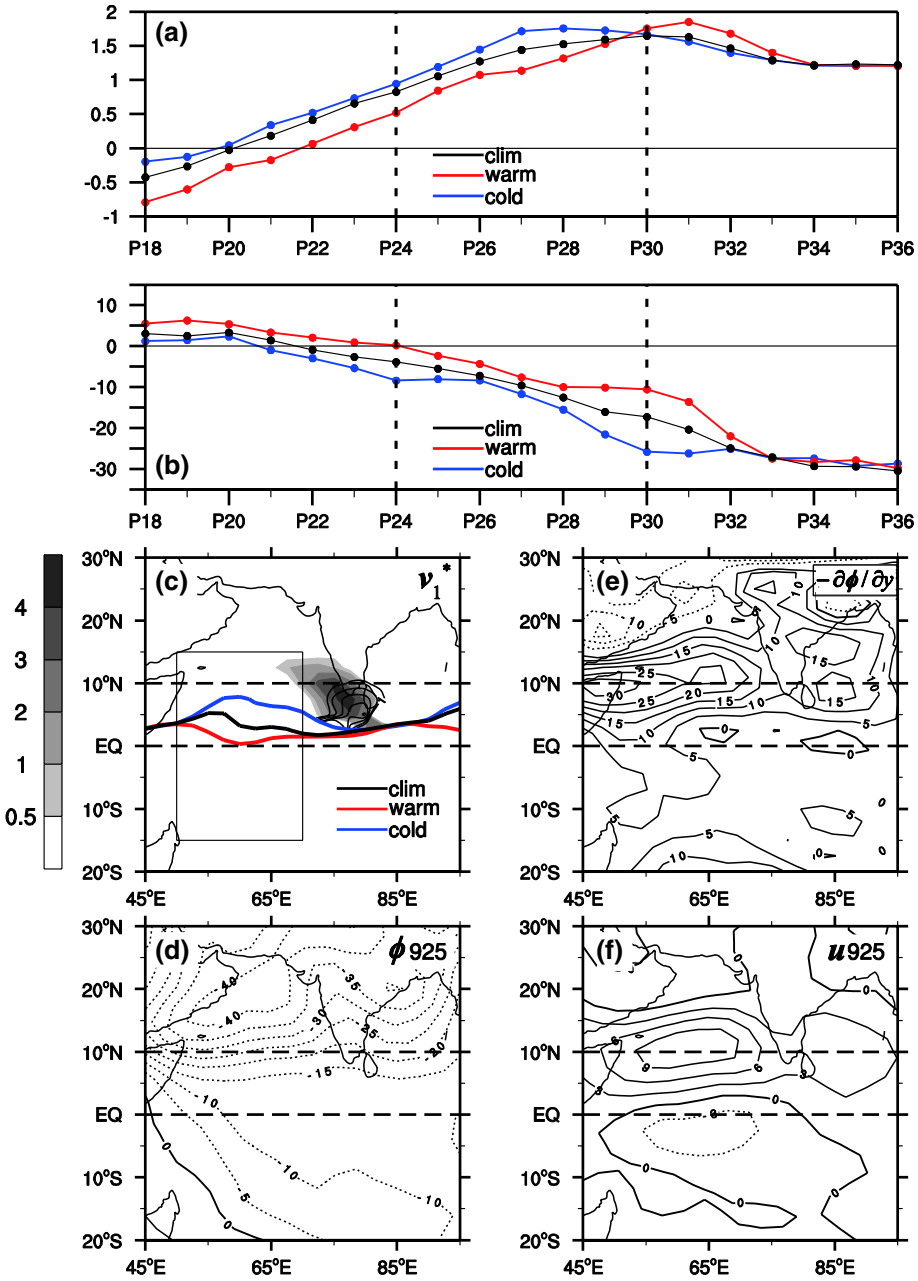

Fig. 11 Temporal evolutions of the cross-equatorial gradient of **a** SST (°C) and **b** 925-hPa geopotential height (gpm) from Pentad 18–36; as well as the 925-hPa horizontal distributions of cold-minus-warm composites at Pentad 30 of **c** zero absolute vorticity contour and v_1^* (*contours*, intervals of 1.0 m s^{-1}), **d** geopotential height (gpm) and **e** its meridional gradient ($-\partial\phi/\partial y$ 10^{-5} m s^{-2}), and **f** zonal wind (m s^{-1}). *Black*, *blue* and *red curves* in (**a**–**c**) represent the climate mean, the cold and warm ENSO composites, respectively; *shading* in (**c**) is for the climatological v_1^* (m s^{-1})

gradient due to the sub-continental land–sea distribution of South Asia. The anomalies of the ageostrophic meridional flow and its convergence then strengthen the forced convection and thus advance the Indian summer monsoon onset.

Under the background of ENSO, the vertically coupled upper- and lower-level circulation anomalies exhibit different features in the onset processes of the BOB and Indian summer monsoon. The anomalous divergence related to the SAH in the upper troposphere during the BOB summer monsoon onset is stronger than that during the Indian summer monsoon onset and is superimposed well with the anomalous convection below. Whereas during the Indian summer monsoon onset, the anomalous lower-level convergence associated with the enhanced inertial instability and forced convection seems to have a more direct effect. It is noteworthy that the anomalies of cross-equatorial SST gradient appear a few weeks before the Indian summer monsoon onset, suggesting that the predictability of Asian summer monsoon onset could be improved if we can verify the threshold of cross-equatorial SST gradient in triggering the monsoon onset convection.

Furthermore, the composite analysis adopted in this study has revealed a linear influence of ENSO on the SASM onset process. However, the nonlinear effects of ENSO, such as changes in the lifecycle and amplitude of ENSO in some years (Hoerling et al. 1997; Slingo and Annamalai 2000), may also affect the SASM onset process.

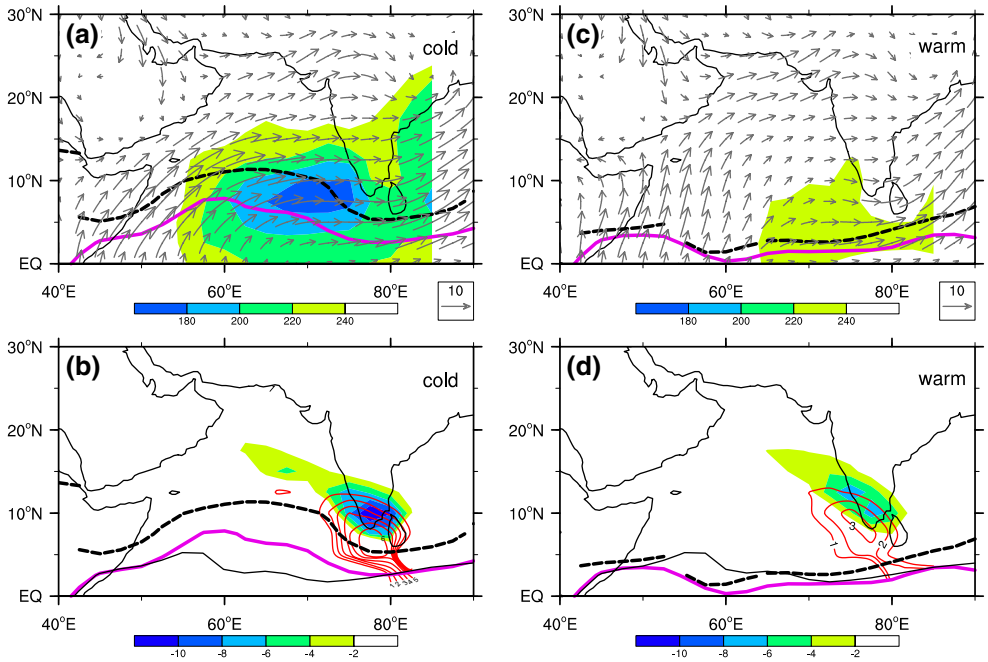

Fig. 12 Composites at Pentad 30 of (**a**, **c**) OLR (*shading*, W m^{-2}) and 925-hPa wind (*vectors*, m s^{-1}); (b, d) the 925-hPa meridional ageostrophic wind $v_1^* \approx -\lambda^2\left(u\frac{\partial}{\partial x}\right)\left(\frac{\partial \phi}{\partial y}\right)$. (*Red contours*, m s^{-1}) and its meridional gradient (*shading*, 10^{-6} s^{-1}) for cold (**a**, **b**) and warm (**c**, **d**) ENSO events. *Pink bold solid* and *black dashed lines* represent the zero absolute vorticity contours and the axis of the westerly maximum, respectively. *Black thin curves* in (**b**) and (**d**) denote the climatological position of zero absolute vorticity contours

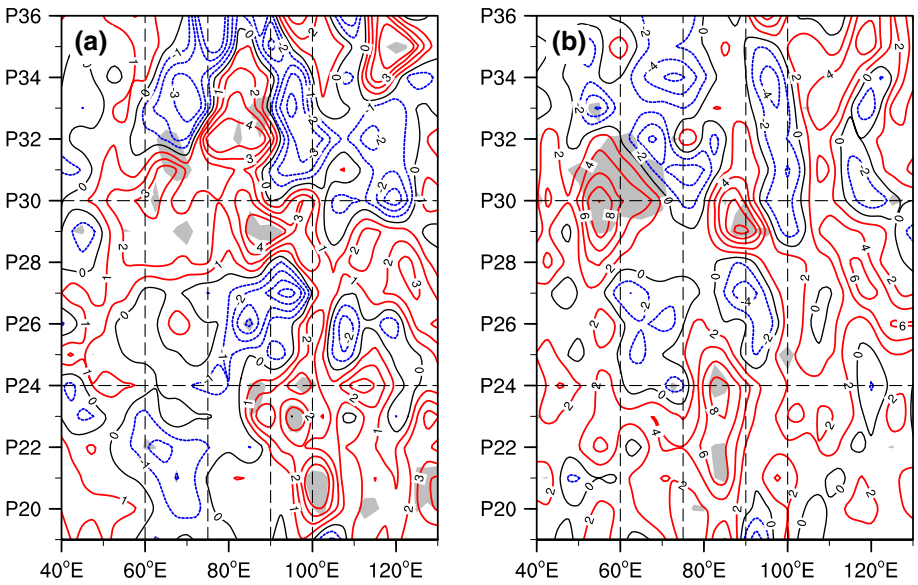

Fig. 13 Time–longitudinal crossing section of cold-minus-warm composites of **a** 150-hPa divergence (10^{-6} s^{-1}) and **b** 850-hPa relative vorticity (10^{-6} s^{-1}) averaged from 5°N to 20°N. *Gray shading* represents the 90 % confidence level of the composites

It is also necessary to point out that, besides ENSO, we cannot ignore the impacts of other external forcing factors, e.g., the thermal forcing of the Tibetan Plateau (Wu and Zhang 1998; Abe et al. 2013), the warm pool in the AS (Sijikumar and Rajeev 2012) and the BOB (Wu et al. 2012) and Indian Ocean Dipole (IOD) (Yuan et al. 2008; Sankar et al. 2011), especially in those years when the early (late) onset of the BOB and Indian summer monsoon takes place without the preceding cold (warm) ENSO events. In boreal spring, the formation of warm pool in the BOB and AS is associated with the ASM onset and can be attributed to the thermal and mechanical forcing of the Tibetan Plateau (Wu et al. 2012; Abe et al. 2013). Recent study (Chakravorty et al. 2013) has shown the relationship between the

meridional gradient of SST anomalies and the cooperation of ENSO and IOD events: the negative gradient of SST anomalies over Indian Ocean in spring is well developed when El Niño co-occurred with positive IOD in preceding year, and only positive IOD cannot lead to the spring meridional gradient of SST anomalies in Indian Ocean. Hence how these factors work together with ENSO in influencing the interannual variability of the Asian summer monsoon onset is subject to further investigations.

Acknowledgments This study was jointly supported by the Chinese Academy of Sciences (XDA11010402), the MOST program (2012CB417203, 2010CB950400), the National Science Foundation of China (41275088, 91337216), and the Project funded by China Postdoctoral Science Foundation (2013M540128).

References

Abe M, Hori M, Yasunari T, Kitoh A (2013) Effects of the Tibetan plateau on the onset of the summer monsoon in South Asia: the role of the air-sea interaction. J Geophys Res Atmos 118:1760–1776

Alexander MA, Blade I, Newman M, Lanzante JR, Lau N-C, Scott JD (2002) The atmospheric bridge: the influence of ENSO teleconnections on air-sea interaction over the global oceans. J Clim 15:2205–2231

Behringer DW, Xue Y (2004) Evaluation of the global ocean data assimilation system at NCEP: The Pacific Ocean. Eighth symposium on integrated observing and assimilation systems for atmosphere, oceans, and land surface, AMS 84th annual meeting, washington state convention and trade center, Seattle, Washington, 11–15

Chakravorty S, Chowdary JS, Gnanaseelan C (2013) Spring asymmetric in the tropical Indian Ocean: role of El Niño and IOD. Clim Dyn 40:1467–1481

Chao WC, Chen B (2001) The origin of monsoons. J Atmos Sci 58:3497–3507

Chen LX, Zhu QG, Luo HB, He JH, Dong M, Feng ZQ (1991) East Asian Monsoon. Meteorology Press, 362 pp

Du Y, Xie SP, Huang G, Hu KM (2009) Role of air–sea interaction in the long persistence of El Niño–induced North Indian Ocean warming. J Clim 22:2023–2038

Gill AE (1980) Some simple solutions for heat-induced tropical circulation. Q J Roy Meteor Soc 106:447–462

Goswami BN (1998) Interannual variations of Indian summer monsoon in GCM: external conditions versus internal feedbacks. J Clim 11:501–522

He JH, Wen M, Wang LJ, Xu HM (2006) Characteristics of the onset of the Asian summer monsoon and the importance of Asian–Australian "land bridge". Adv Atmos Sci 23:951–963

Hoerling MP, Kumar A, Zhong M (1997) El Niño, La Niña, and the nonlinearity of their teleconnections. J Clim 10:1769–1786

Joseph PV, Eischeid JK, Pyle RJ (1994) Interannual variability of the onset of Indian summer monsoon and its association with atmospheric features, El Nino, and sea surface temperature anomalies. J Clim 7:81–105

Ju JH, Slingo JM (1995) The Asian summer monsoon and ENSO. Q J Roy Meteor Soc 121:1133–1168

Kanamitsu M, Ebisuzaki W, Woollen J, Yang S-K, Hnilo JJ, Fiorino M, Potter GL (2002) NCEP-DOE AMIP-II reanalysis (R-2). Bull Am Meteorol Soc 83:1631–1643

Kawamura R (1998) A possible mechanism of the Asian summer monsoon-ENSO coupling. J Meteorol Soc Japan 76:1009–1027

Klein SA, Soden BJ, Lau N-C (1999) Remote sea surface temperature variations during ENSO: evidence for a tropical atmospheric bridge. J Clim 12:917–932

Krishnamurti TN, Ardanuy P, Ramanathan Y, Pasch R (1981) On the onset vortex of the summer monsoons. Mon Wea Rev 109:344–363

Lau N-C, Nath MJ (2003) Atmophere–ocean variations in the Indo-Pacific sector during ENSO episodes. J Clim 16:3–20

Lau N-C, Nath MJ (2012) A model study of the air-sea interaction associated with the climatological aspects and interannual variability of the South Asian summer monsoon development. J Clim 25:839–857

Li Qian, RenRC CaiM, Wu GX (2012) Attribution of the summer warming since 1970s in Indian Ocean Basin to the inter-decadal change in the seasonal timing of El Niño decay phase. Geophys Res Lett 39:L12702. doi:10.1029/2012GL052150

Liebmann B, Smith CA (1996) Description of a complete (interpolated) outgoing longwave radiation dataset. Bull Am Meteorol Soc 77:1275–1277

Liu YY, Ding YH (2008) Teleconnetcion between the Indian summer monsoon onset and the Meiyu over the Yangtze River Valley. Sci China Ser D-Earth Sci 51:1021–1035

Liu BQ, Wu GX, Mao JY, He JH (2013) Genesis of the South Asian high and its impact on the Asian summer monsoon onset. J Clim 26:2976–2991

Liu BQ, Liu YM, Wu GX, Yan JH, He JH, Ren SL (2014) Asian summer monsoon onset barrier and its formation mechanism. Clim Dyn. doi:10.1007/s00382-014-2296-0

Mao JY (2001) Variation in the configuration of Subtropical Anticyclone during seasonal transition and the Mechanism of Asian monsoon onset. Ph.D. dissertation, Graduate University of Chinese Academy of Sciences (in Chinese)

Mao JY, Wu GX (2007) Interannual variability in the onset of the summer monsoon over the Eastern Bay of Bengal. Theor Appl Climatol 89:155–170

Mao JY, Wu GX (2011) Barotropic process contributing to the formation and growth of Tropical Cyclone Nargis. Adv Atmos Sci 28:1–9

Mao JY, Chan JCL, Wu GX (2004) Relationship between the onset of the South China Sea summer monsoon and the structure of the Asian subtropical anticyclone. J Meteorol Soc Jpn 82:845–849

Mason RB, Anderson C (1958) The development and decay of the 100mb summertime anticyclone over southern Asia. Mon Wea rev 91:3–12

Meehl GA (1994) Influence of the land surface in the Asian summer monsoon: external conditions versus internal feedbacks. J Clim 7:1033–1049

Meng W, Wu GX (2000) Gearing between the indo-monsoon circulation/Pacific-walker circulation and ENSO, Part II: simulation. Chin J Atmos Sci (in Chinese) 24:15–25

Miyakoda K, Kinter JL, Yang S (2003) The role of NESO in the South Asian monsoon and pre-monsoon signals over the Tibetan plateau. J Meteorol Soc Jpn 81:1015–1039

Okumura YM, Deser C (2010) Asymmetry in the duration of El Niño and La Niña. J Clim 23:5826–5843

Reynolds RW, Rayner NA, Smith TM, Stokes DC, Wang W (2002) An improved in situ and satellite SST analysis for climate. J Clim 15:1609–1625

Sankar S, Ramesh Kumar MR, Reason C (2011) On the relative roles of El Niño and Indian Ocean Dipole events on the monsoon onset over Kerala. Theor Appl Climatol 103:359–374

Sijikumar S, Rajeev K (2012) Role of the Arabian Sea warm pool on the precipitation characteristics during the monsoon onset period. J Clim 25:1890–1899

Slingo JM, Annamalai H (2000) 1997: the El Niño of the century and the response of the Indian summer monsoon. Mon Wea Rev 128:1778–1797

Soman MK, Slingo JM (1997) Sensitivity of the Asian summer monsoon-aspects of sea-surface-temperature anomalies in the tropical Pacific Ocean. Q J Roy Meteor Soc 123:309–336

Tao SY, Chen LX (1987) A review of recent advances in research on Asian monsoon in China. In: Chang CP, Krishnamurti TN (eds) Monsoon meteorology. Oxford University Press, London, pp 60–92

Tomas RA, Webster PJ (1997) The role of inertial instability in determining the location and strength of near-equatorial convection. Q J R Meteorol Soc 123:1445–1482

Tomas RA, Holton JR, Webster PJ (1999) The influence of cross-equatorial pressure gradients on the location of near-equatorial convection. Q J Roy Meteor Soc 125:1107–1127

Wang B, Lin H (2002) Rainy season of the Asian-Pacific summer monsoon. J Clim 15:386–398

Wang B, Wu RG, Fu XH (2000) Pacific-East Asian teleconnection: how does ENSO affect East Asian climate? J Clim 13:1517–1536

Webster PJ, Yang S (1992) Monsoon and ENSO, selectively interactive systems. Q J Roy Meteor Soc 118:877–926

Webster PJ, Magaña VO, Palmer TN, Shukla J, Tomas RA, Yanai M, Yasunari T (1998) Monsoons: processes, predictability, and the prospects of prediction. J Geophys Res 103:14451–14510

Wu GX, Zhang YS (1998) Tibetan Plateau forcing and the timing of the monsoon onset over South Asian and the South China Sea. Mon Weather Rev 126:913–927

Wu GX, Liu BQ (2014) Roles of forced and inertially unstable convection development in the onset process of Indian summer monsoon. Sci China Earth Sci 57:1438–1451

Wu GX, Meng W (1998) Gearing between the Indo-monsoon circulation and the Pacific-Walker circulation and the ENSO. Part I: data analyses. Chin J Atmos Sci (in Chinese) 22:470–480

Wu RG, Kirtman BP, Krishnamurthy V (2008) An asymmetric mode of tropical Indian Ocean rainfall variability in boreal spring. J Geophys Res 113. doi:10.1029/2007JD009316

Wu GX, Guan Y, Liu YM, Yan JH, Mao JY (2012) Air-sea interaction and formation of the Asian summer monsoon onset vortex over the Bay of Bengal. Clim Dyn 38:261–279

Xie SP (1996) Westward propagation of latitudinal asymmetry in a coupled ocean-atmosphere model. J Atmos Sci 53:3236–3250

Xie SP, Annamalai H, Schott FA, McCreary JP (2002) Structure and mechanisms of South Indian Ocean climate variability. J Clim 15:864–878

Yanai M, Esbensen S, Chu JH (1973) Determination of bulk properties of tropical cloud clusters from large–scale heat and moisture budgets. J Atmos Sci 30:611–627

Yang S, Lau K-M (1998) Influences of sea surface temperature and ground wetness on Asian summer monsoon. J Clim 11:3230–3246

Yang S, Lau K-M, Yoo S-H, Kinter JL, Miyakoda K, Ho C-H (2004) Upstream subtropical signals preceding the Asian summer monsoon circulation. J Clim 17:4213–4229

Yang X, Yao T, Yang W, Xu B, He Y, Qu D (2012) Isotopic signal of earlier summer monsoon onset in the Bay of Bengal. J Clim 25:2509–2516

Yasunari T, Seki Y (1992) Role of the Asian monsoon on the interannual variability of the global climate system. J Meteorol Soc Jpn 70:177–188

Yuan Y, Yang H, Zhou W, Li CY (2008) Influences of the Indian Ocean dipole on the Asian summer monsoon in the following year. Int J Climatol 28:1849–1859

Zhang RH, Sumi A (2002) Moisture circulation over East Asia during El Nino episode in Northern winter, spring and autumn. J Meteorol Soc Jpn 80:213–227

Zhang RH, Sumi A, Kimoto M (1999) A diagnostic study of the impact of El Nino on the precipitation in China. Adv Atmos Sci 16:229–241

Zhang HM, Bates JJ, Reynolds RW (2006) Assessment of composite global sampling: sea surface wind speed. Geophys Res Lett 33:L17714. doi:10.1029/2006GL027086

Zhang YN, Wu GX, Liu YM, Guan Y (2014) The effects of asymmetric potential vorticity forcing on the instability of South Asia high and Indian summer monsoon onset. Sci China Earth Sci 57:337–350